

A Comparative Study of MEMS Microactuators for Use in a Dual-stage Servo with an Instrumented Suspension

Xinghui Huang, *Student Member, IEEE*, Roberto Horowitz, *Member, IEEE*, and Yunfeng Li, *Member, IEEE*

Abstract—This paper presents the design and analysis of a dual-stage servo system with an instrumented suspension for use in hard disk drives (HDDs). The dual-stage system is equipped with a MEMS microactuator (MA), either rotational or translational, as a secondary actuator. In both cases, the MA has a resonance mode at 2.2 kHz and has virtually no other modes up to 40 kHz. Two design approaches, the sensitivity decoupling design and the multi-objective optimization, are applied in the design of the servo system. With either approach, the translational dual-stage actuator achieves better tracking performance than the rotational one by about 13%, which is achieved mainly by attenuating airflow-excited suspension vibrations. This improvement is significant when the servo system's track misregistration (TMR) budget approaches the level of 5-10 nanometers, in which airflow-excited suspension vibration has become a significant contribution to TMR.

Index Terms—Hard Disk Drives, Microactuators, Servo Control, Vibration Control.

I. INTRODUCTION

THE increase of data track density in hard disk drives (HDDs) is possible only when the position accuracy of the read/write head can be improved accordingly. For example, at the targeted track density of 500k tracks per inch (TPI), the allowable track misregistration (TMR) is about 5 nm (3σ value). In order to satisfy higher requirements of position accuracy, it is necessary to develop high-bandwidth, robust track-following servo systems. Dual-stage actuators have thus been proposed and explored intensively as a means of attaining the necessary servo bandwidth to achieve the required compensation of track runout and rejection of various disturbances. In a dual-stage configuration, a secondary actuator is added on to the conventional voice coil motor (VCM) in order to offer better mechanics and faster dynamic responses to compensate for high-frequency disturbances.

Although there have been many possible configurations for the secondary actuator, two popular approaches are currently

Manuscript received April 27, 2005; revised January 6, 2006. This work was supported by the Information Storage Industry Consortium (INSIC) and the Computer Mechanics Laboratory (CML) of the University of California at Berkeley.

X. Huang was with the Department of Mechanical Engineering, University of California, Berkeley. He is now with Seagate Research, 1251 Waterfront Place, Pittsburgh, PA 15222 USA (e-mail: xinghui.huang@seagate.com).

R. Horowitz is with the Department of Mechanical Engineering, University of California, Berkeley, CA 94720 USA, (e-mail: horowitz@me.berkeley.edu).

Y. Li is with Samsung Information System America (e-mail: yunfeng.li@sisa.samsung.com).

Publisher Item Identifier S 0000-0000(06)00000-0

being considered by the disk drive industry and researchers. The first approach is called the actuated suspension type [1][2], in which a piezoelectric device is placed on the suspension to flex the suspension around a pivot. The second approach is called the actuated slider type [3][4], in which an electrostatic MEMS microactuator (MA) is sandwiched between the gimbal and the slider, and it either rotates or translates the slider relative to the suspension tip. The actuated slider approach results in a truly collocated system without exciting the structural resonance modes of the suspension. Besides, the microactuator usually has very clean dynamic responses: it has a single mass-spring mode in the frequency range of 1-3 kHz, and there are no other significant modes up to 40 kHz [5][4][6]. With MEMS fabrication and integration techniques, the MEMS MA can be batch-fabricated and micro-assembled with the head and gimbal on the suspension. All these features associated with the actuated slider approach provide the potential for forming high-performance servo systems.

There are two types of MEMS MAs: rotational [3] and translational [4][6]. In the rotational MA case, the actuation of the VCM and MA can be viewed as being decoupled with each other, i.e., each actuator contributes to the head motion independently, resulting in a truly parallel structure. This feature eases the design of servo controllers, especially when the relative motion output of the MA is measurable [7][8] with embedded capacitive sensors. In the translational MA case, the VCM actuation can excite MA dynamics, resulting in a coupled dual-stage actuator. Any motion at the suspension tip, especially those airflow-induced suspension vibrations, will pass through the mass-spring system of the MA and get filtered before affecting the head motion. This feature is desirable as the allowable TMR is approaching 3σ 5 nm, where airflow-induced suspension vibration has become a significant contribution to TMR.

Besides the use of dual-stage actuators for achieving higher servo bandwidth, instrumented suspensions have also been proposed as a means of providing information on airflow-induced suspension vibration [9][10][11]. The sensor output can be used for VCM/suspension mode damping to improve its bandwidth [9], or be used for feedforward vibration compensation [10], or both [11]. This signal can be sampled at a higher rate than that of the position error signal (PES) in order to deal with the high-frequency property of suspension vibrations.

Several controller design methods have been proposed for

MEMS-based dual-stage servo systems, which can be roughly categorized into two major categories. The first includes those methodologies that utilize sequential single-input single-output (SISO) frequency shaping design techniques, such as the PQ method [12] and the sensitivity decoupling method [13][7]. The second includes those multivariable optimal control design techniques such as μ -synthesis [14] and mixed H_2/H_∞ [11].

This paper presents the design and analysis of a dual-stage servo system with an instrumented suspension. Both rotational and translational MEMS MAs are considered as a secondary actuator. Two design approaches are employed: the sensitivity decoupling approach and the mixed H_2/H_∞ approach. The difference between rotational and translational MAs and its impact on controller design and system performance are analyzed in detail. Simulation results are presented to verify those observations. This paper is organized as follows. Section 2 gives a general model for a MEMS MA dual-stage actuator with an instrumented suspension. Detailed controller design is discussed in Sections 2-4 respectively. Section 5 gives the simulation results and comparative analysis. Conclusions are provided in Section 6.

II. PLANT SETUP AND MODELLING

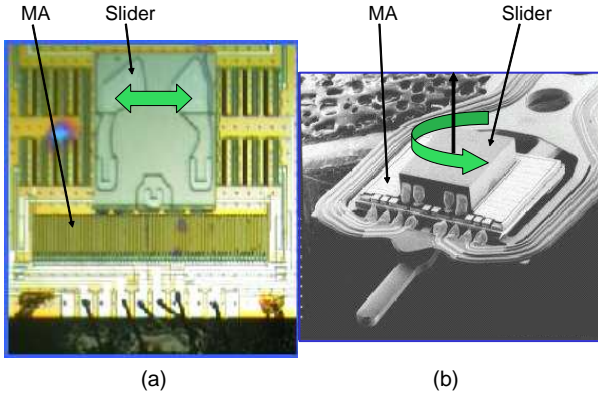


Fig. 1. (a) Berkeley's translational MA (courtesy of K. Oldham), (b) HGST's rotational MA (courtesy of M. White)

Fig. 1 shows the SEM photo of a translational and a rotational MAs. The mechanisms and block diagram of the two dual-stage actuators are illustrated in Figs. 2 and 3 respectively. The frequency responses of the translational dual-stage actuator are shown in Fig. 4. In these figures, u_v and u_m are the control inputs to the VCM and MA respectively. w_a is airflow turbulence acting on the suspension, by which suspension resonance modes are excited. y_h , y_p , y_m , and y_v are the read/write head position, the strain sensor output, the relative motion output of the MA, and the suspension tip position, respectively. In conventional disk drive systems, only y_h is available in the form of the PES when the plant is closed by a tracking controller. In dual-stage actuators with a MEMS MA and an instrumented suspension, y_p and y_m are measurable from the strain sensor on the suspension surface and the capacitive sensing embedded in the MA respectively. In all cases, y_v is not measurable.

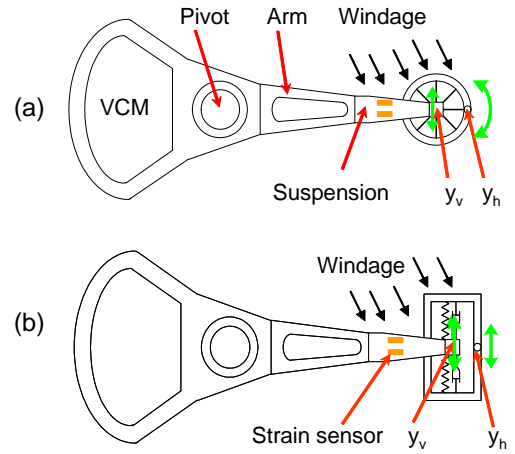


Fig. 2. Mechanisms of translational and rotational MAs

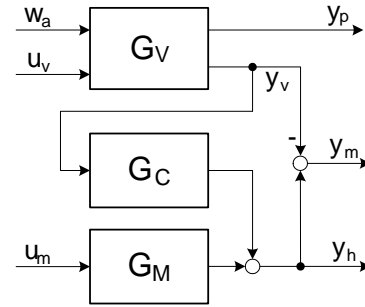


Fig. 3. Block diagram for dual-stage actuators with an instrumented suspension

G_V is the dynamics of the VCM-suspension assembly from u_v to y_v , and its transfer function is

$$G_V(s) = \frac{A_0}{s^2} + \sum_{i=1}^N \frac{A_i}{s^2 + 2\zeta_i\omega_i s + \omega_i^2}. \quad (1)$$

In this model, G_V consists of a rigid body mode, a major sway mode at 7.4 kHz, or called the butterfly mode, and five suspension resonance modes at 5.1 kHz, 9.1 kHz, 10.7 kHz, 13 kHz and 15 kHz, respectively. All these resonance modes have a slight damping coefficient of about 0.015 N·s/m. During operation, high-speed airflow turbulence in the disk drive enclosure acts on the suspension and excites suspension vibrations. G_M is the dynamics of the MA from u_m to y_h , either rotational or translational, and its transfer function is

$$G_M(s) = \frac{A_m}{s^2 + 2\zeta_m\omega_m s + \omega_m^2}. \quad (2)$$

It has been modelled as a single spring-mass-damper system with $\omega_m=2.2$ kHz and $\zeta_m=0.2$ N·s/m.

G_C is the coupling dynamics from y_v to y_h . When the MA is rotational, G_C is constantly one, then y_m is solely the output of the MA driven by u_m , implying virtually no coupling between the VCM and MA [7]. This decoupling effect mainly results from the fact that the translational motion of the suspension tip passes through the MA's center of mass,

resulting in no rotational motion of the MA. On the other hand, when the MA is translational, we have a coupled dual-stage system. G_C is then derived from the MA dynamics and can be expressed as

$$G_C(s) = \frac{2\zeta_m\omega_m s + \omega_m^2}{s^2 + 2\zeta_m\omega_m s + \omega_m^2}. \quad (3)$$

This coupling effect implies that actuation of the VCM will excite the dynamics of the MA, and y_m becomes the combined output of u_v and u_m . In both cases, rotational and translational, actuation of the MA can be assumed to have little effect on the VCM dynamics due to the very small inertia of the MA compared to that of the VCM. This assumption implies that the transfer function from u_m to y_p is constantly zero.

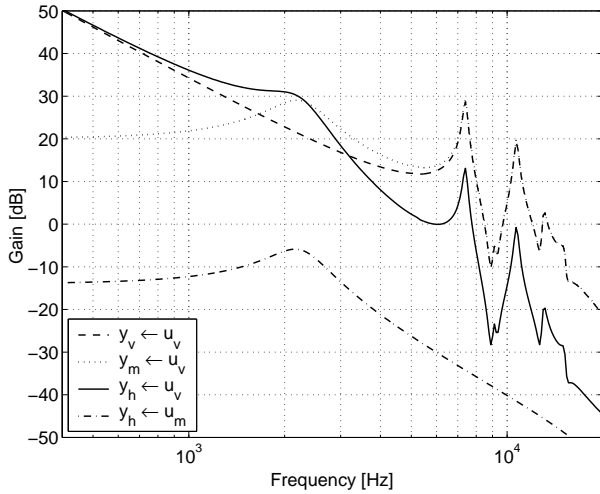


Fig. 4. Frequency responses of the dual-stage actuator

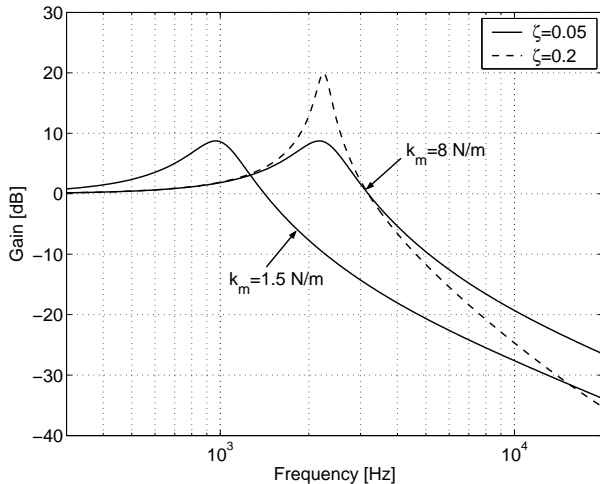


Fig. 5. Frequency responses of the coupling dynamics G_C

In the translational MA case, the coupling dynamics exhibit a low-pass filtering effect, as shown in Fig. 5. It can be seen that both the spring stiffness k_m and the damping coefficient c_m can affect the filtering effect. This effect makes a difference between the rotational and translational MAs. From the viewpoint of suspension vibration attenuation, we

would like to have a soft spring and a light damping effect, such that most high-frequency suspension vibrations can be attenuated when passing through the MA. On the other hand, we want large values for k_m and c_m so that the transfer function from u_v to y_h has high gains in a wide frequency range for effective track-following control. Therefore tradeoff is necessary between vibration attenuation and track following. From Fig. 5 we see that, when $\omega_m=2.2$ kHz and $\zeta_m = 0.2$, the gain of G_C is above zero decibel up to 3 kHz, implying little degradation of the actuation gain of the VCM-suspension assembly in the low-frequency range for track following, and adequate filtering in the high-frequency range for suspension vibration attenuation.

III. MINOR LOOP DESIGN OF VIBRATION DAMPING AND COMPENSATION

When y_p and y_m are available as auxiliary information, it is possible to first design some minor loop vibration damping controllers before designing an outer loop tracking controller. Besides, the two signals can be sampled at a higher rate than that of the PES so as to achieve better control effects.

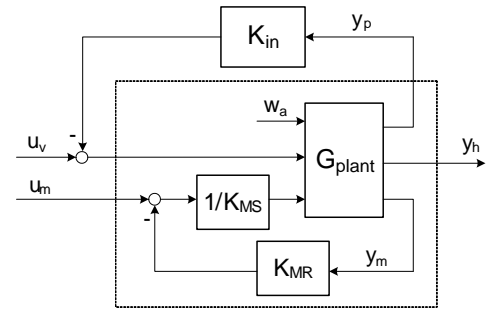


Fig. 6. Minor loop vibration damping and compensation

A. MA Damping Control

The basic use of the relative motion signal, y_m , is to actively damp the microactuator resonance mode to make for a well-behaved MA and to simplify the control design that follows. This can be implemented as a minor loop around the MA as shown in the lower part of Fig. 6. To begin with, the MA plant is first discretized using the zero-order hold at 50 kHz:

$$G_M(q^{-1}) = \frac{q^{-1}B_o(q^{-1})}{A_o(q^{-1})}, \quad (4)$$

where q^{-1} is the one-step delay operator. The desired damped MA can be expressed as

$$G_{MD}(q^{-1}) = \frac{q^{-1}B_o(q^{-1})}{A_D(q^{-1})}. \quad (5)$$

This can be achieved by solving the following Diophantine equation

$$A_D(q^{-1}) = A_o(q^{-1})K_{MS}(q^{-1}) + q^{-1}B_o(q^{-1})K_{MR}(q^{-1}). \quad (6)$$

The closed-loop polynomial $A_D(q^{-1})$ is chosen by the designer and usually the damping coefficient for G_{MD} is set to be one.

B. Suspension Vibration Control

After the minor loop around the MA is closed, a vibration controller K_{in} is designed using y_p to provide some damping of the suspension resonance modes. The design of K_{in} is formulated as a standard LQG problem. Consider the discrete-time representation of the plant with the MA damped, which is shown in the dashed box in Fig. 6:

$$\begin{aligned} x(k+1) &= Ax(k) + Bu(k) + B_w w_a(k), \\ y(k) &= Cx(k) + n(k), \end{aligned} \quad (7)$$

where $y(k) = [y_h(k) \ y_p(k)]^T$, $u(k)$ is the control input to the VCM, and the airflow turbulence $w_a(k)$ and measurement noise $n(k)$ are random signals with zero mean. In this model for controller design, only three major suspension modes are considered in order to restrain the designed controller order. The goal of designing K_{in} is to minimize the cost function

$$J = E \{ y_h^2(k) + Ru^2(k) \}, \quad (8)$$

where $E\{\cdot\}$ is the expectation operator and R is the control weighting.

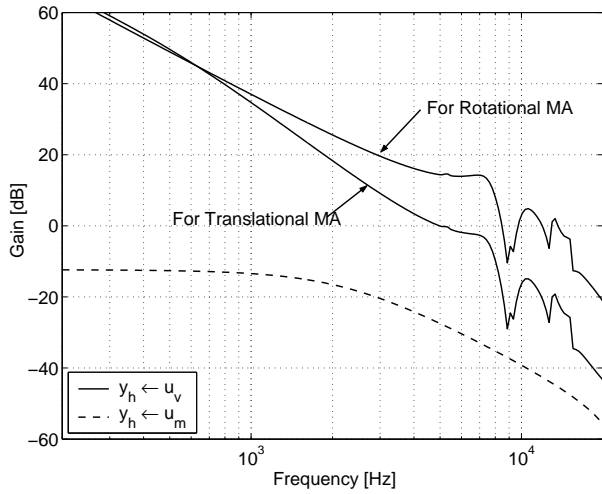


Fig. 7. Frequency responses of the damped plant

Fig. 7 shows the frequency responses of the two damped plants. Two major resonance modes of the VCM and the MA mode are damped by using y_p and y_m , respectively. As can be seen, the frequency response from u_v to y_h for the translational MA case has stronger high-frequency attenuation than that for the rotational MA case due to the coupling effect. This implies that the translational MA will behave better in suspension vibration attenuation which mainly happens in the high-frequency range.

IV. SENSITIVITY DECOUPLING DESIGN

The decoupling control approach, originally introduced by [13], is popularly applied in the design of track-following controllers for dual-stage servos. This approach utilizes the PES and y_m to generate the position error of the suspension tip relative to the data track center, which will be labelled as VPES

$$VPES = PES + y_m = r - y_v, \quad (9)$$

and this signal is then fed to the VCM loop controller K_V . With this configuration as shown in Fig. 8(a), the decoupling design of K_V and K_M is made possible: the VCM loop and the MA loop can be designed sequentially using conventional SISO design techniques.

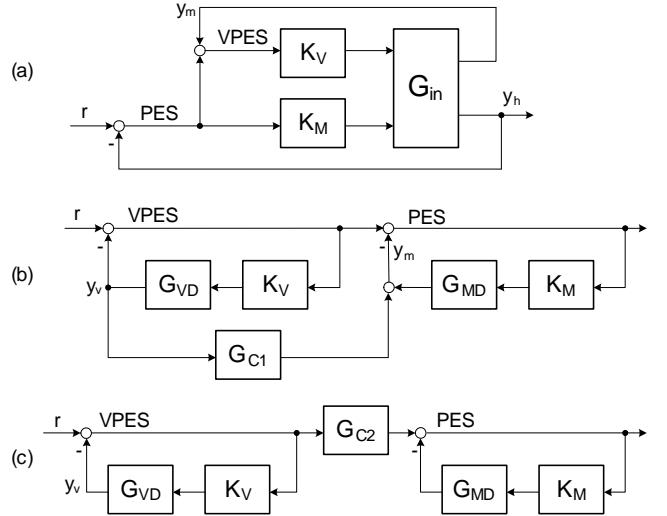


Fig. 8. Block diagram of sensitivity decoupling design

$$G_{C1} = \frac{K_{MS}}{K_{MS} + G_M K_{MR}} (G_C - 1), \quad (10)$$

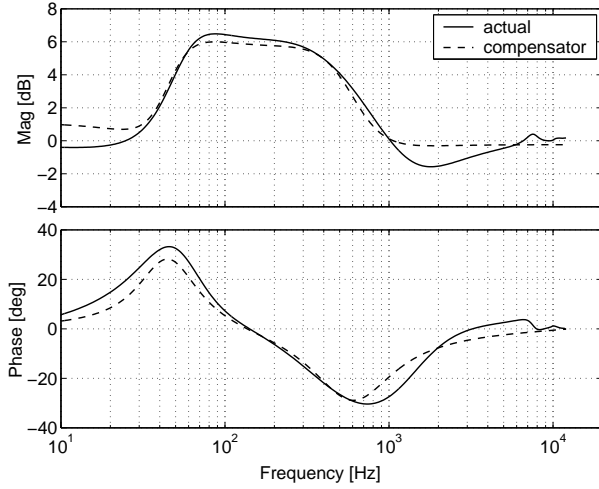
$$G_{C2} = 1 - G_{C1} G_V K_V. \quad (11)$$

It is worthwhile to pay specific attention to the coupling effect in this design process. The blocks G_{C1} and G_{C2} in Fig. 8 are derived from the coupling effect G_C as shown in Fig. 3 and (3). As can be seen, for a rotational MA, $G_C = 1$, then $G_{C1} = 0$ and $G_{C2} = 1$, implying exact decoupling between the two minor loops in Fig. 8(c). In the translational MA case, G_{C2} involves all plant dynamics and controllers designed except for K_M . The frequency response of G_{C2} is shown in Fig. 9. It is seen that the dynamics of G_{C2} is fairly mild: it is about 6 dB in the region 60-500 Hz, and close to zero decibel beyond 1 kHz. Its phase property is mild as well: 30 degrees around 60 Hz and -30 degrees around 600 Hz. This implies that based on the K_M designed for the rotational MA case, a modifier which has the similar dynamics to G_{C2} can be designed to compensate for the coupling effect, yielding a sensitivity response similar to that of the rotational MA case:

$$K_{MC} = K_M K_C \approx K_M G_{C2}, \quad (12)$$

where K_M is the controller designed for the rotational MA case, K_C is the modifier to compensate for G_{C2} , and its dynamics are also shown in Fig. 9 in dashed lines.

In the rotational MA case, the design of K_V and K_M is to use pole placement. The reader is referred to [7] for more details. In this paper, K_V is designed to achieve a closed-loop bandwidth of 600 Hz for the VCM loop, and K_M achieves a closed-loop bandwidth of 3 kHz for the MA loop. The final sensitivity is the product of the two and it achieves a closed-loop bandwidth of 2.4 kHz. Their frequency responses are


 Fig. 9. Frequency responses of G_{C2} and compensator K_C

shown in Fig. 10, and the comparison between the designs for rotational and translational MAs is shown in Fig. 11.

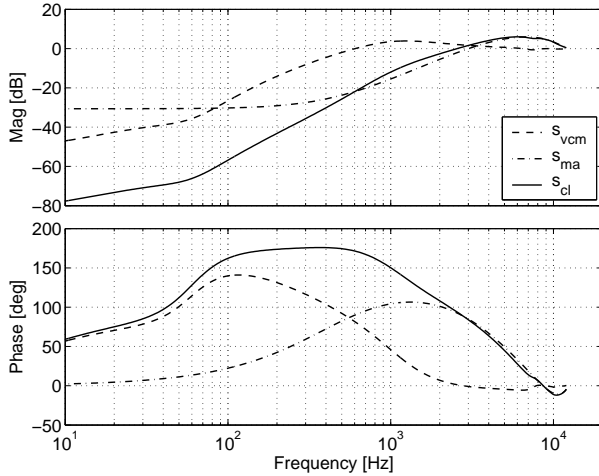


Fig. 10. Sensitivities of the decoupling design with a rotational MA

V. MULTI-OBJECTIVE OPTIMIZATION THROUGH LMIS

In this section, a multi-objective optimization method, or called the mixed H_2/H_∞ approach, is applied to the design of tracking controllers. Unlike the sensitivity decoupling approach, which proceeds sequentially by SISO design methods, the mixed H_2/H_∞ approach is a MIMO design approach. It formulates the optimization of tracking performance as an H_2 control problem, and stability robustness is explicitly considered by posing some H_∞ norm bounds. Fig. 12 shows the schematic for this method. Its design procedure is briefly explained below and the reader is referred to [11] for more details.

In Fig. 12, G_{RO} is the frequency shaping function for generating the track runout from the normalized noise w_r . A third-order function is used to approximate the real signal:

$$G_{RO}(s) = \frac{7.8 \times 10^9}{s^2 + 800s + 2.5 \times 10^5} + \frac{1.2 \times 10^5}{s + 1.9 \times 10^3}. \quad (13)$$

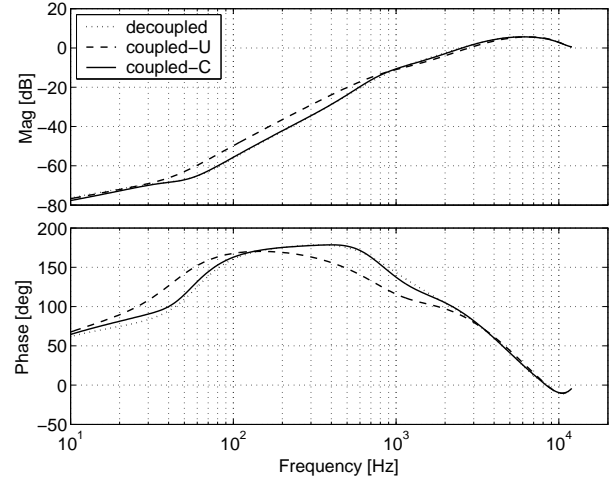


Fig. 11. Comparison of sensitivities for rotational and translational MAs. “decoupled”: original design for the rotational MA case; “coupled-U”: the same controllers applied to the translational MA case without compensation by K_C ; “coupled-C”: the system is compensated by K_C .

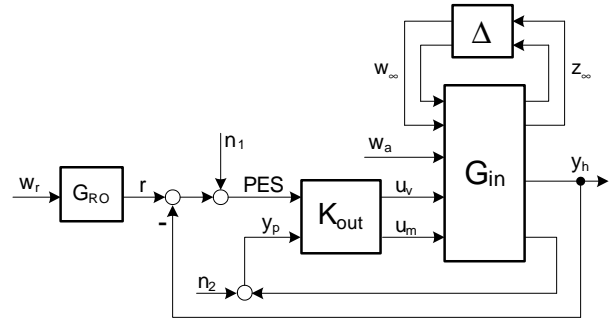


Fig. 12. Block diagram for multi-objective optimization method

The RMS value of this runout is about 450 nm in the range of 10 Hz-25 kHz. G_{in} is the plant with MA damping and K_{in} closed, as shown in Fig. 6. Δ_V and Δ_M are the multiplicative uncertainties of the nominal actuator model:

$$\begin{aligned} G_V(s) &= G_{Vnom}(s)(1 + \Delta_V(s)W_V(s)), \\ G_M(s) &= G_{Mnom}(s)(1 + \Delta_M(s)W_M(s)). \end{aligned} \quad (14)$$

Here, G_{Vnom} and G_{Mnom} are the nominal dynamics of the VCM and MA respectively, $\|\Delta_V\|_\infty \leq 1$, $\|\Delta_M\|_\infty \leq 1$, and W_V and W_M are the magnitude bounding functions of the two uncertainties:

$$\begin{aligned} W_V(s) &= \frac{3s^2 + 3 \times 10^4 s + 1.4 \times 10^8}{s^2 + 4.6 \times 10^4 s + 1.4 \times 10^9}, \\ W_M(s) &= \frac{s + 6.28 \times 10^3}{s + 6.28 \times 10^4}. \end{aligned} \quad (15)$$

The first design criterion is expressed as to minimize the RMS value of the PES, or equivalently, the H_2 norm of the transfer function from disturbances to the PES:

$$\min \text{RMS}(PES) \Leftrightarrow \min \|G_{z_2 w_2}\|_2, \quad (16)$$

where $z_2 = [PES \ u_v \ u_m]^T$ and $w_2 = [w_r \ w_a \ n_1 \ n_2]^T$. Stability robustness of the closed-loop system is characterized

by the structured singular value [15]:

$$\sup_{\omega} \mu_{\Delta}(G_{cl}(j\omega)) < 1, \quad (17)$$

where $\Delta = \text{diag}[\Delta_V, \Delta_M]$, and G_{cl} is the closed-loop plant with K_{out} closed around G_{in} .

Since the dimension of the Δ block is only 2, condition (17) can be approximated by setting μ -bounds on the two uncertain channels separately, that is, $\sup \mu_{\Delta_V}(G_{cl}(j\omega)) < \gamma_V$ and $\sup \mu_{\Delta_M}(G_{cl}(j\omega)) < \gamma_M$, with γ_V and γ_M strictly less than 1. They can be further reduced to $\|G_{\Delta_V}\|_{\infty} < \gamma_V$ and $\|G_{\Delta_M}\|_{\infty} < \gamma_M$ when Δ_V and Δ_M are scalars.

From the above discussion, we have shown that the multi-objective optimization problem can be cast as an H_2 minimization problem with some H_{∞} bounds, i.e., to design an output dynamic feedback controller K_{out} such that

$$K_{out} = \arg \min_{K_{out}} \gamma_2, \quad (18)$$

$$\text{with } \|G_{z_2 w_2}\|_2 < \gamma_2, \quad (19)$$

$$\|G_{z_{\infty} w_{\infty, \Delta_V}}\|_{\infty} < \gamma_V, \quad (20)$$

$$\text{and } \|G_{z_{\infty} w_{\infty, \Delta_M}}\|_{\infty} < \gamma_M. \quad (21)$$

This minimization problem with inequalities can be transformed to a set of LMIs and be solved with some convex optimization algorithm [16].

It is noted that this approach can be applied to dual-stage servo designs with either a rotational or translational MA, because this approach is a MIMO design method and does not rely on the specific structure of the plant. As an example, the frequency response of K_{out} for the translational MA case, from the PES to u_v , is shown in Fig. 13. From the figure we see that when H_{∞} bounds are imposed, the controller gain in the high-frequency range is reduced significantly compared to the H_2 design in order to achieve more stability margin. Hankel model reduction technique is then applied to reduce the controller order from 21 to 14 with little dynamics variation.

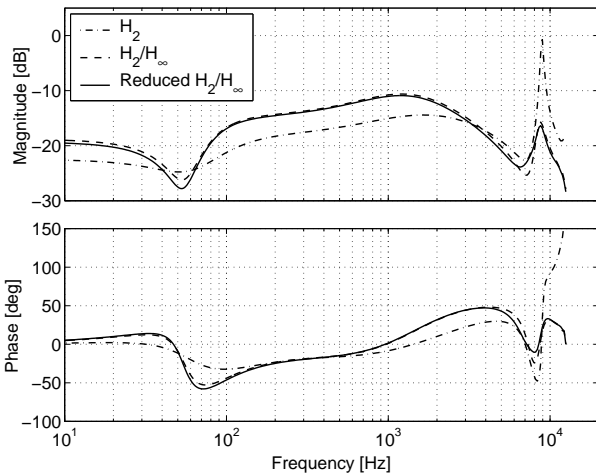


Fig. 13. Bode plots for K_{out} . H_2 : H_2 norm minimization only, which is equivalent to the LQG design; H_2/H_{∞} : multi-objective design with H_{∞} bounds; Reduced H_2/H_{∞} : reduced-order controller of the second one.

VI. ADAPTIVE FEEDFORWARD COMPENSATION FOR SUSPENSION VIBRATION

As mentioned before, some suspension resonance modes can be damped by using the strain signal y_p measured from the suspension surface. Actually this signal can further be exploited to drive the MA to compensate for the airflow-excited suspension vibrations appearing at y_h [17].

Define G_{wp} and G_{wh} to be the transfer functions from w_a to y_p and y_h respectively. We want the feedforward compensator, K_{MF} , to minimize the airflow-excited vibrations at the head, i.e., to minimize

$$e_a = G_M K_{MF} G_{wp} w_a + G_{wh} w_a. \quad (22)$$

This mechanism is different from the feedback damping of the VCM in that, the motion generated by the MA cannot directly affect the suspension outputs, y_v and y_p . Therefore, what it can do is to compensate for those vibrations at the head that result from suspension vibration. It is also desirable to tune the coefficients of the feedforward compensator in real time in order to take into account variations in the suspension dynamics and the airflow turbulence characteristics.

In this paper, K_{MF} assumes the form of finite impulse response (FIR) for stability consideration:

$$K_{MF}(\theta, q^{-1}) = h_0 + h_1 q^{-1} + \dots + h_n q^{-n}, \quad (23)$$

where θ is the filter coefficient vector $\theta = [h_0 \ h_1 \ \dots \ h_n]^T$ and n is the order of K_{MF} . The feedforward compensation motion can be expressed as

$$\begin{aligned} y_{MF}(k) &= G_M(q^{-1}) K_{MF}(q^{-1}) y_p(k) \\ &= K_{MF}(q^{-1}) G_M(q^{-1}) y_p(k) \\ &= K_{MF}(q^{-1}) x_f(k) \\ &= \theta^T \phi(k-1), \end{aligned} \quad (24)$$

where $x_f(k) = G_M(q^{-1}) y_p(k)$, $\phi(k) = [x_f(k) \ x_f(k-1) \ \dots \ x_f(k-n)]^T$. Since $x_f(k)$ is not measurable, it is estimated by passing $y_p(k)$ through the model of the MA, \hat{G}_M :

$$x_f(k) = \hat{G}_M(q^{-1}) y_p(k). \quad (25)$$

The coefficients of θ are tuned in such a way that $E\{e_a^2(k)\}$ is minimized. However, e_a is not directly measurable. What we have is the PES, and it can be written as

$$PES(k) = e_a(k) + e_r(k), \quad (26)$$

where e_r represents the tracking error resulting from all other disturbance sources except for the airflow turbulence acting on the suspension. It is roughly valid to assume that w_a and r are uncorrelated, then we have

$$E\{PES^2(k)\} = E\{e_a^2(k)\} + E\{e_r^2(k)\}. \quad (27)$$

Thus, minimizing $E\{e_a^2(k)\}$ is equivalent to minimizing $E\{PES^2(k)\}$, and we can use the PES as a corrupted error signal to perform the adaptation. With e_a corrupted by e_r , there will be some degradation in feedforward compensation performance, and a little longer time is expected for the adaptation process to converge.

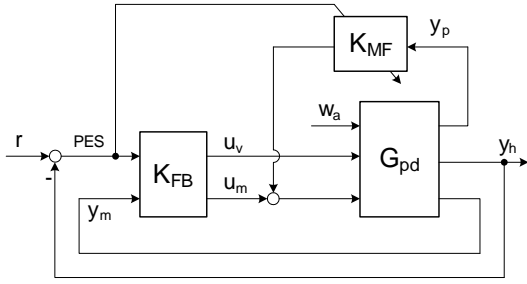


Fig. 14. Block diagram of adaptive feedforward compensation

It is noted that, adaptive feedforward compensation does not affect the stability property of the already designed and closed feedback system, since it is an add-on part and aims at minimizing the RMS value of the PES by generating additional motion at the MA to compensate for it. Therefore, the vibration compensation part can be implemented on any already-stabilized closed-loop system. It is also expected that feedforward compensation will be more useful in the rotational MA case than in the translational case, since the suspension vibration at y_v will equally show up at y_h without any mechanical attenuation. These observations will be verified by the simulation results in the next section.

VII. SIMULATION RESULTS

Simulations are conducted to investigate the performance of systems with different structures and controllers. In simulation, the reference signal r is generated from a combination of various sources, such as repeatable track runout, disk flutter, low-frequency torque disturbances to the VCM, etc. The plant can be either rotational or translational, as illustrated in Fig. 3. To account for parametric uncertainty in the plant, the adaptive feedforward compensator, K_{MF} , is implemented along with a fixed feedback controller K_{FB} , which is designed either by sensitivity decoupling or by LMI optimization. Measurement noises are injected into the system at proper locations. The strain sensor signal assumes a signal-to-noise ratio of 35 dB. The measurement noise levels of the relative motion of the MA and the PES are 1 nm and 2 nm (RMS value), respectively.

Fig. 15 shows the simulation results for various configurations, in which FF means adaptive feedforward compensation of the MA using y_p . Comparing (a) and (c), we can see significant differences between the rotational and translational MAs, especially in the high-frequency range. There are almost no resonance modes showing up in (c) due to the coupling, or filtering, effect. Comparing (a) and (b), we see that the LMI design achieves better performance than the decoupling design by optimally shaping the sensitivity function and making a better balance between the attenuation of r and w_a . From (c) and (d), we can see more clearly the improvement by optimal shaping.

Table I summarizes the simulation results in more detail. In the table, the total PES has been decomposed into two parts: $PES(w_a)$ and $PES(r)$, where $PES(w_a)$ is the PES resulting from airflow turbulence, and $PES(r)$ donates the remaining PES resulting from all other disturbance sources

TABLE II
PARAMETER VARIATIONS OF PLANT RESONANCE MODES

Parameters	Variations		
	Minus	Nominal	Plus
VCM natural frequency (ω_i)	-10%	0	+10%
MA natural frequency (ω_m)	-15%	0	+15%
Damping coefficient (ζ_i, ζ_m)	-20%	0	+20%
Modal constant (A_i, A_m)	- 5%	0	+ 5%

including measurement noise. With this decomposition, we can more clearly see the improvement by adaptive feedforward compensation. In the table, R and T denote the rotational and translational plant cases respectively. Two aforementioned design methods are employed: the sensitivity decoupling design and the LMI design. Under plant parameter variation, three plant situations are considered: minus, nominal and plus. They indicate how much the plant's modal parameters vary as specified in Tab. II, where those parameters were defined in Eqs. 1-3. Those values expressed in percentage indicate how much improvement that is achieved by adaptive feedforward compensation compared to the cases without FF as shown in the left columns.

Several conclusions can be drawn from Table I.

- 1) The translational MA case always performs better than the rotational MA case in the attenuation of airflow-excited suspension vibrations, no matter what kind of design approach is used. We also see that this improvement is mainly achieved by reducing $PES(w_a)$ with little change in $PES(r)$. Obviously this is due to the mechanical, or passive, filtering effect of the translational MA on suspension vibration.
- 2) The LMI design achieves better performance than the decoupling design by better balancing the attenuation of $PES(r)$ and $PES(w_a)$. For the R-N case, both $PES(r)$ and $PES(w_a)$ are reduced by the LMI design, while for the T-N case, the LMI design reduces $PES(r)$ significantly by amplifying $PES(w_a)$ a little, resulting in a smaller total PES. This trend can also be seen from Fig. 15. A better balance between $PES(r)$ and $PES(w_a)$ implies that the final PES becomes closer to a white noise and there is less room for further reduction.
- 3) Adaptive feedforward compensation can further attenuate $PES(w_a)$, especially when there is plant variation. The effectiveness of feedforward compensation is affected by several factors: the order, or the tap number, of the compensator K_{MF} , the sampling rate of y_p , and the SNR of y_p . With a higher sampling rate, the compensator will be more effective in dealing with high-frequency resonance modes. During practical implementation, the strain sensor may pick up some resonance modes that do not contribute to the head offtrack motion. These modes are called non-offtrack modes and in feedforward compensation, they just appear as measurement noise to deteriorate the compensation performance. Optimization in sensor location and orientation is therefore necessary to improve the SNR for better vibration compensation [18].
- 4) The combination of the LMI design and adaptive feed-

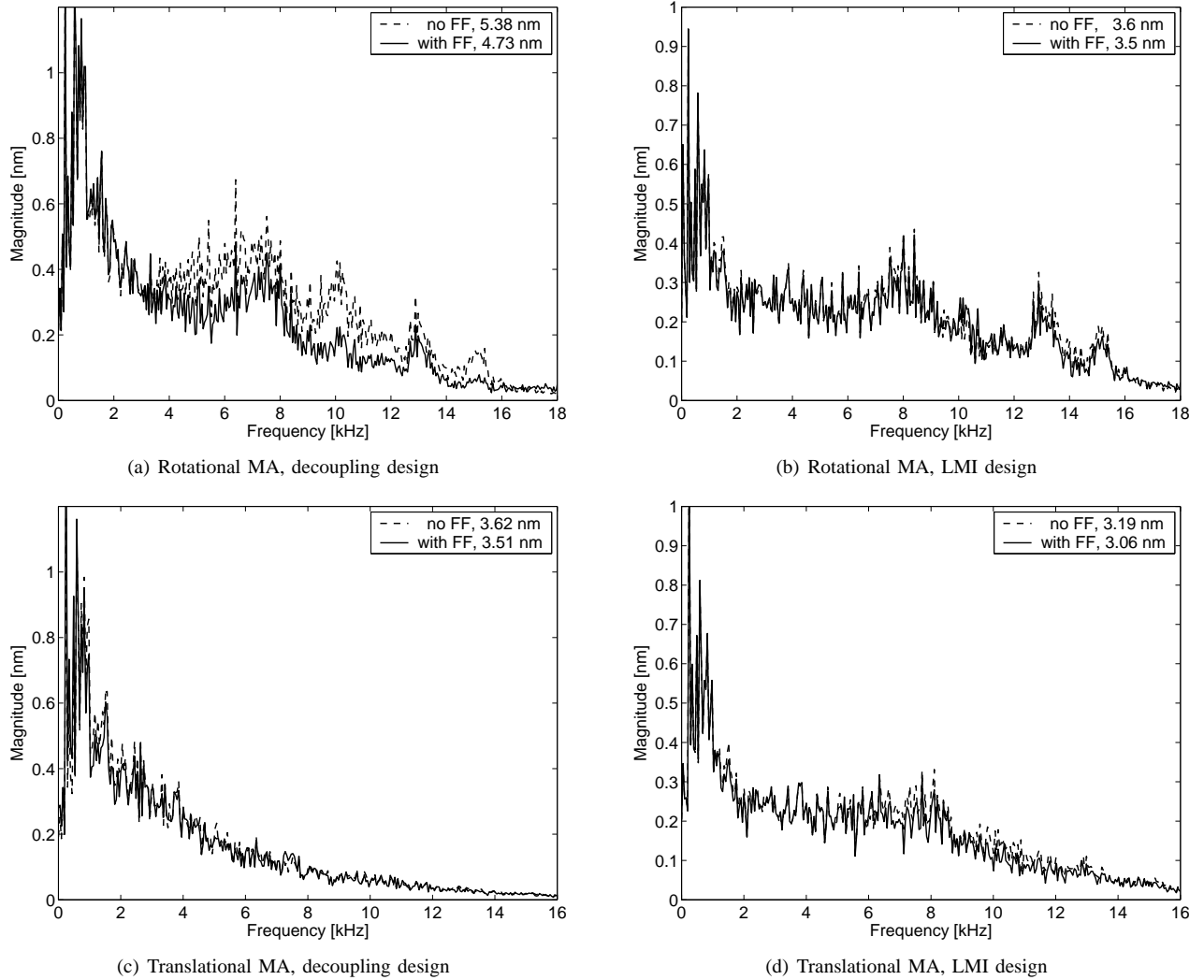


Fig. 15. Power spectra of the PES for various system configurations

TABLE I
PERFORMANCE COMPARISON BETWEEN VARIOUS PLANTS AND CONTROL DESIGNS

Plant type	Parameter variation	Tracking controller	PES(r) [nm]		PES(w_a) [nm]		total PES [nm]	
			no FF	with FF	no FF	with FF	no FF	with FF
R	N	Decp	3.62	3.57	3.98	3.10 (22%)	5.38	4.73 (12%)
T	N	Decp	3.49	3.51	0.96	0.65 (32%)	3.62	3.57 (2%)
R	M	LMI	2.75	2.73	2.75	2.53 (8%)	3.89	3.72 (5%)
R	N	LMI	2.77	2.74	2.32	2.18 (6%)	3.61	3.50 (3%)
R	P	LMI	2.99	2.93	2.46	2.09 (15%)	3.87	3.60 (7%)
T	M	LMI	2.81	2.82	1.90	1.40 (26%)	3.39	3.15 (7%)
T	N	LMI	2.78	2.78	1.56	1.28 (18%)	3.19	3.06 (4%)
T	P	LMI	2.81	2.79	1.67	1.35 (19%)	3.27	3.10 (5%)

forward compensation can achieve the best performance with fairly good performance robustness. For the rotational MA case, performance degradation under plant variation is less than 6%, while this degradation is less than 3% for the translational MA case. Again, the translational MA case achieves better performance robustness partially due to the coupling-filtering effect, which is very robust to parameter variation.

Some points should be noted on the simulation results

shown here. The disturbance model used in the simulation is based on the results from a single-stage system, which may differ from that of a dual-stage system when an MA is added. The MA resonance mode may be excited directly by airflow turbulence. But with the relative MA motion available for inner loop damping, this effect can be greatly reduced. Sensing noise is also an important issue. The claimed system performance relies on good sensing properties with a high signal-to-noise ratio of y_m [8].

VIII. CONCLUSION

This paper has explored the difference between rotational and translational MEMS MAs for use in dual-stage servo systems and the resulting effect on the attenuation of airflow-excited suspension vibrations. Due to the inherent coupling effect between the major and secondary actuators for the translational MA case, airflow-excited suspension vibrations can be naturally attenuated, which eases the design of vibration attenuation and servo control. If properly chosen, the resonance frequency of the translational MA can make a good tradeoff between a high gain of $G_{y_h \leftarrow u_v}$ in the low-frequency range for tracking control, and enough vibration attenuation in the high-frequency range.

Two servo control design approaches have been explored: the sensitivity decoupling design and the mixed H_2/H_∞ design through LMI. The sensitivity decoupling design yields a set of sequential SISO controllers of low orders, which are straightforward to design and implement. In the LMI design, stability robustness is explicitly taken into account by incorporating some H_∞ bounds with respect to the plant's multiplicative uncertainties.

Simulation results showed that the translational MA is beneficial to vibration attenuation. The LMI design achieves better performance by better balancing the attenuation of $PES(r)$ and $PES(w_a)$. Adaptive feedforward compensation can achieve further attenuation of $PES(w_a)$ and exhibits good performance robustness under plant variation.

REFERENCES

- [1] R. Evans, J. Griesbach, and W. Messner, "Piezoelectric microactuator for dual stage control," *IEEE Trans. Magnetics*, vol. 35, no. 2, pp. 977–982, 1999.
- [2] S. Arya, Y.-S. Lee, W.-M. Lu, M. Staudenmann, and M. Hatchett, "Piezo-based milliactuator on a partially etched suspension," *IEEE Trans. Magnetics*, vol. 37, no. 2, pp. 934–939, March 2001.
- [3] T. Hirano, M. White, H. Yang, K. Scott, S. Pattanaik, S. Arya, and F.-Y. Huang, "A moving-slider mems actuator for high-bandwidth hdd tracking," in *Proc. Intermag*, vol. 3, Anaheim, CA, 2003, pp. 2535–2540.
- [4] D. Horsley, N. Wongkomet, R. Horowitz, and A. Pisano, "Precision positioning using a microfabricated electrostatic actuator," *IEEE Trans. Magnetics*, vol. 35, no. 2, pp. 993–999, March 1999.
- [5] T. Hirano, L.-S. Fan, W. Lee, J. Hong, W. Imano, S. Pattanaik, S. Chan, R. Horowitz, S. Aggarwal, and D. Horsley, "High-bandwidth high-accuracy rotary microactuators for magnetic disk drive tracking servos," *IEEE/ASME Trans. Mechatronics*, vol. 3, pp. 156–165, Sept. 1998.
- [6] K. Oldham, X. Huang, and R. Horowitz, "Design, fabrication, and control of a high-aspect ratio microactuator for vibration suppression in a hard disk drive," in *Proc. 16th IFAC World Congress*, Prague, Czech, July 2005.
- [7] Y. Li and R. Horowitz, "Mechatronics of electrostatic microactuators for computer disk drive dual-stage servo systems," *IEEE/ASME Trans. Mechatronics*, vol. 6, no. 2, pp. 111–121, 2001.
- [8] M. T. White and T. Hirano, "Use of relative position signal for microactuators in hard disk drives," in *Proc. Amer. Control Conf.*, Denver, CO, June 2003, pp. 2535–2540.
- [9] Y. Huang, M. Banther, P. D. Mathur, and W. Messner, "Design and analysis of a high bandwidth disk drive servo system using an instrumented suspension," *IEEE/ASME Trans. Mechatronics*, vol. 4, no. 2, pp. 196–206, 1999.

- [10] Y. Li, F. Marcassa, R. Horowitz, R. Oboe, and R. Evans, "Track-following control with active vibration damping of a PZT-actuated suspension dual-stage servo system," in *Proc. Amer. Control Conf.*, Denver, CO, June 2003, pp. 2553–2559.
- [11] X. Huang, R. Nagamune, R. Horowitz, and Y. Li, "Design and analysis of a dual-stage disk drive servo system using an instrumented suspension," in *Proc. Amer. Control Conf.*, Boston, MA, June 2004, pp. 535–540.
- [12] S. J. Schroeck and W. C. Messner, "On controller design for linear time-invariant dual-input single-output systems," in *Proc. Amer. Control Conf.*, San Diego, CA, June 1999, pp. 4122–4126.
- [13] K. Mori, T. Munemoto, H. Otsuki, Y. Yamaguchi, and K. Akagi, "A dual-stage magnetic disk drive actuator using a piezoelectric device for a high track density," *IEEE Trans. Magnetics*, vol. 27, no. 6, pp. 5298–5300, Nov. 1991.
- [14] D. Hernandez, S.-S. Park, R. Horowitz, and A. K. Packard, "Dual-stage track-following servo design for hard disk drives," in *Proc. Amer. Control Conf.*, San Diego, CA, June 1999, pp. 4188–4121.
- [15] G. J. Balas, J. C. Doyle, K. Glover, A. Packard, and R. Smith, *μ -Analysis and Synthesis Toolbox for use with MATLAB*. MUSYN Inc. and The MathWorks, Inc., USA, 1995.
- [16] J. F. Sturm, *Using Sedumi 1.05, A MATLAB Toolbox for Optimization over Symmetric Cones*, 2001.
- [17] Y. Li and R. Horowitz, "Active suspension vibration control with dual-stage actuators in hard disk drives," in *Proc. Amer. Control Conf.*, Arlington, VA, June 2001, pp. 2786–2791.
- [18] K. Oldham, S. Kon, and R. Horowitz, "Fabrication and optimal strain sensor placement in an instrumented disk drive suspension for vibration suppression," CML Blue Report, Dept. of Mechanical Engineering, U. C. Berkeley, Tech. Rep. 10, Oct. 2003.



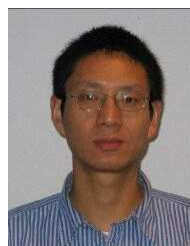
Xinghui Huang (S'05) received the B.S. and M.S. degrees from Tsinghua University, Beijing, China, in 1994 and 1999, and a Ph.D. degree in 2006 in mechanical engineering from the University of California at Berkeley. He joined the Seagate Research as a research staff member recently.

His research interests include vibration control, adaptive control, robust control, multirate control, and mechatronics with applications to disk drive servo.



Roberto Horowitz Venezuela in 1955. He received a B.S. degree with highest honors in 1978 and a Ph.D. degree in 1983 in mechanical engineering from the University of California at Berkeley.

In 1982 he joined the Department of Mechanical Engineering at the University of California at Berkeley, where he is currently a Professor and Vice Chair of graduate Studies. Dr. Horowitz teaches and conducts research in the areas of adaptive, learning, nonlinear and optimal control, with applications to Micro-Electromechanical Systems (MEMS), computer disk file systems, robotics, mechatronics and Intelligent Vehicle and Highway Systems (IVHS). Dr. Horowitz is a member of IEEE and ASME.



Yunfeng Li (S'01-M'03) received the B.S. and M.S. degrees in Manufacturing Engineering from Beijing University of Aeronautics and Astronautics, Beijing, China, in 1992 and 1995, respectively, and the Ph.D. degree in Mechanical Engineering from University of California at Berkeley in 2003. He is currently working in the disk drive servo control area at Samsung Information Systems America. Prior to that, he worked as a servo engineer at Maxtor Corporation.